Journal of Building Engineering, Volume 66, May 2023, Article Number 105865
DOI: 10.1016/j.jobe.2023.105865

Dynamic response-based crack resistance analysis of fibre reinforced concrete beams under different temperatures and crack depths

Abstract

Steel fibre-reinforced concrete has been used extensively because of its excellent mechanical properties. Academic researchers have comprehensively discussed the impact and challenges of fibre reinforcement to obtain optimal properties in the resultant concrete. Most researchers reported the mechanical performance of fibre-reinforced concrete (FRC) under static loads. A few studies did conclude the mentioned performance on dynamic loads. However, a comprehensive analysis is still missing that can explain the crack resistance performance of FRC under dynamic loads at relatively high temperatures. In this study, the efficacy of FRC beams for crack resistance is analysed under coupled loads, i.e., dynamic load at relatively high temperatures as compared to room temperature. Various researchers found that concrete's qualities may change at different temperatures due to moisture content, physical and chemical changes to the ingredients, differences in cooling and heating schedules, water-to-cement ratio, and aggregate. The rate of reduction in moisture content is quite possible even in relatively high temperatures as compared to standard room temperature. Therefore, we selected a range of temperature that demonstrate tests on more realistic weather conditions for most of the concrete applications. As per theory, a slight change in modulus or strength shall definitely effect the dynamic response. Therefore, we tested cantilever FRC beams on a modal excitor in a band heater to expose the beams to bending loads at different temperature values. The variation in the beam's dynamic response parameters, including modal amplitude and frequency, is discussed, and compared with experimental results for regular and reinforced concrete beams. The SIF of plain concrete decreased as concrete temperature increased. Compared to conventional concrete, using SFRC-1 enhanced fracture resistance by 10-20% at various crack depths (2mm, 4mm, 6mm) and temperatures (20 °C, 40°C, 60°C).

NOMENCLATURE

a	Crack depth
A	Beam section
A_L, A_R	Coefficients
b	Beam width
B	Coefficient
B_L, B_R	Coefficients
C_L, C_R	Coefficients
D_L, D_R	Coefficients
E	Elastic modulus
E_0	Elastic modulus at T_0
f	Frequency
$f_r(a/H)$	Shape function

H	Beam thickness
I	Area moment of inertia
J_z	Momentum of inertia
k	Torsional spring stiffness
l	Distance between the crack location and fixed end of the beam
L	Beam length
m	End mass
m_{acc}	Accelerometer mass
ω	Angular frequency
ω_s	Angular frequency of a shaker
$q_n(t)$	Modal coordinate of the n-th mode
ρ	Density
t	Time
$T(t)$	Modal coordinate
U_0	Shaker displacement amplitude
x	Distance to the fixed end of the beam
$y(x,t)$	Beam displacement due to bending
$y_L(x,t)$	Fixed-end side beam displacement
$y_R(x,t)$	Free-end side beam displacement
$Y(x,t)$	Mode shape of the beam
$Y_n(x)$	n-th mode shape of the beam
SIF	Stress intensity factor
SFRC	Steel fibre reinforced concrete

1.Introduction

A crack in a structure, in general, affects local stiffness and influences dynamic structural responses, such as displacement amplitudes, natural frequencies, and mode shapes. These dynamic responses include information about the size and location of the crack(s). Many studies have concentrated on the vibration properties of the cracked beams [1–3]. Ostachowicz and Krawczuk, for example, calculated the natural frequencies of double-sided cracks and single-sided cantilever beams by modelling a crack as a torsional spring model [4]. According to the experimental and analytical results, the natural frequency of the cantilever beam reduced as the crack increased. Studies have also been conducted to examine the dynamic response of a cantilever beam using a fracture mechanics-derived spring stiffness model [5–11]. However, a torsional spring model can only describe superficial cracks. Some investigations have studied the relationship between crack propagation and natural frequency [5,9,12–16]. The location and extent of damage can be estimated using mode shapes [6,17–19]. Other researchers claimed that variations in curvature modes may be used to determine a crack [20–22]. Mode shapes and natural frequencies of cracked aluminium cantilever beams were investigated by Zai et al. [23]. In their work, Khan et al. computed the fundamental frequency of a non-prismatic aluminium 1050 cantilever beam at various temperatures and found that the elastic modulus changed to represent the changing ambient temperature [24]. Numerical, analytical and empirical studies have revealed that increasing the temperature results in a lower structural natural frequency. Several additional investigations [2] came to the same conclusion. Gupta et al., for example, studied the fundamental frequency of a thermally cracked isotropic aluminium microplate. The effect of the thermal environment was evaluated in terms of temperature-induced moments and in-plane forces [25]. Gillich et al. proposed a multi-modal damage detection approach in fluctuating temperature situations[15]. The internal load was calculated since a fixed steel beam was used.

Significantly, the investigations mentioned above focused on metal materials, and only a few studies have been undertaken to examine the vibration response of cracked fibre-reinforced concrete (FRC) beams. Concrete constructions are more likely to be subjected to temperature and dynamic stresses. As a result, the mechanical characteristics of concrete structures are improved by adding fibres of various materials to reinforce them. However, most of these estimates are produced through empirical testing and quasi-static conditions [26–42]. In recent decades, FRC has been studied for improved crack control. When fibres are combined with concrete, it increases the load-bearing capacity as well as the crack resistance. [43]. Today, concrete is recognized as one of the most important and universal building materials due to its capacity to withstand compressive load, temperature resistance, and durability[44].

In addition, composite concrete structures play an essential role in enhancing load-bearing capacity due to their multifunctional properties, i.e., superior strength, energy absorption, and durability [45–47]. Other researchers observed that short-term data from most durability investigations [48] showed that GFRP bars exhibited a considerable loss in mechanical attributes, primarily tensile strength. As a result, it increases the overall service life of the FRC-based structure. However, there is very little literature available that can provide a quantitative assessment of the mentioned increase in crack resistance.

Concrete's mechanical properties are significantly impacted by temperature variations brought on by the hydration process in bulk concrete or by changes in the environment. Therefore, mechanical characteristics must be considered when designing concrete structures[49–51]. For these reasons, it is required to research and quantify how temperature and aging affect concrete properties. Several studies on the degradation of concrete when exposed to extreme temperatures have been conducted. Concrete structures may be subjected to high-temperature changes, coincidental causes, or auxiliary application characteristics, and as a result, concrete changes may influence their mechanical characteristics [52]. Various researchers found that Concrete's qualities may change at different temperatures due to moisture content, physical and chemical changes to the ingredients, differences in cooling and heating schedules, water-to-cement ratio, and aggregates[53–55]. Because of its high fatigue strength, fibre-reinforced concrete (FRC) is commonly utilized in the construction of bridges and underground structures (tunnels), as well as in improving/reinforcing structures subjected to earthquake forces[56–59]. The dynamic compressive strength and elastic modulus of Fiber reinforced reduce as temperature rises, while critical strain rises. Furthermore, peak toughness rises first and then falls within the same conditions[60]. Developing a dynamic response model for FRC is critical to account for thermomechanical loads accurately and accurately reflecting actual working environments. Structural behaviour of the crack’s resistance is quite significant for concrete applications.

The stress intensity factor represents the crack resistance and fracture toughness of a material [61,62]. The crucial stress intensity factor for concrete mixture grades and the impact of different factors on it were experimentally determined in [63–65].The stress intensity factor explicitly states the increase in intensity at the crack's tip; the crack would then propagate when it exceeds the material's toughness. Both fracture growth and crack opening (the rise of the fracture surface displacement) could boost the permeability of concrete, resulting in a loss in cement integrity. Designers and engineers can use the factor of stress intensity as an essential input variable to predict the durability of materials cracked under various failure modes [64]. As a result, some research has focused on concrete design, concentrating on fracture mechanics to obtain more detailed results [65].

In this study, the efficacy of FRC beams for crack resistance is analyzed under coupled loads i.e., dynamic load at relatively high temperatures. Cantilever FRC beams were tested on a modal excitor in a band heater to expose the beams with bending loads at different temperature values. The variation in

beam's dynamic response parameters, including modal amplitude and frequency, is discussed, and compared with experimental results for regular and reinforced concrete beams. The stress intensity factor (SIF) and displacement amplitude characteristics show that the steel fibre-reinforced concrete specimens have excellent ductile behaviour and higher crack resistance than ordinary concrete samples.

2. Experimental Methodology

The analytical models presented in Section 3 should be appropriately validated. As a result, appropriate experiments were devised to consider dynamic thermomechanical loads. The chosen test parameters were specified, and an experimental setup was created to monitor structural integrity and dynamic response during a fatigue life test. In the analytical models, the temperature-dependent Young's modulus value was also calculated.

2.1 Materials

This investigation used Portland EMC II composite cement and standard coarse and fine aggregates (Table 1). A sieve evaluation of the aggregates used revealed that they were appropriate for making the concrete mixture. Flowaid SCC superplasticizer was added to enhance the workability of the concrete, making it more usable and flowable. The concrete was workable, with good cohesion, negligible segregation, and no bleed water. The mix concrete design and Novocon® FE-1050 steel fibres at a 1% amount were used in this study, in accordance with Khalel and Khan's optimization study of fibres Table 2 explain fibre properties. The table 1 shown the mixing percentages of the control concrete.

Table 1 Mixing percentages of the control concrete

Quantity	Cement (kg)	Water (L)	Fine aggregate (kg)	Coarse aggregate (kg)
Per m^3	427	213	679	1061
Trial mix 0.009 m^3	3.843	1.917	6.273	9.549
Superplasticizer (0.5% form cement)	0.0192 kg for trial mix			

Table-2 Fibre properties.

Type of fibre	Shape	Diameter (mm)	Length of fibre (mm)	Tensile strength of fibre (N/mm^2)	Supplier
SFRC-1	Straight	1	20	1150	Sika

2.2 Experimental Design and Procedure

2.2.1 Geometry of the Cantilever Beam

Figure 1 shows the geometry of the cantilever beam used in the experiment. The beam was 25 mm thick. An initial seeded crack with widths and depths of 2 mm, 4 mm, and 6 mm was present on the top surface, close to the fixed end of the beam, to achieve maximum stress concentration. The seeded crack was measured at 5 mm from the fixed end of the beam. The free end of the beam was fitted with an

extra-lightweight accelerometer (mass: 0.6 g) from PCB® (Depew, NY, USA). Table 3 shows the number of experiments was done in this study.

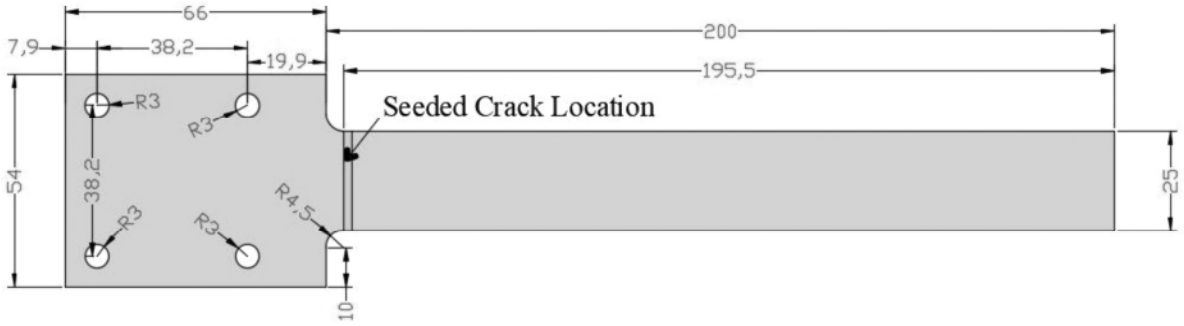

Figure-1 Geometry of a beam with dimensions of 200 mm, 30 mm, and 25 mm.

Table 3 Experimental scheme

Mix type	Crack depth (mm)	Temperatures (°C)	Number of samples test for each Temperature	Test number for each crack dept
Control Mix	0	(20,40,60)	(3,3,3)	9
Control Mix	2	(20,40,60)	(3,3,3)	9
Control Mix	4	(20,40,60)	(3,3,3)	9
Control Mix	6	(20,40,60)	(3,3,3)	9
SFRC	0	(20,40,60)	(3,3,3)	9
SFRC	2	(20,40,60)	(3,3,3)	9
SFRC	4	(20,40,60)	(3,3,3)	9
SFRC	6	(20,40,60)	(3,3,3)	9
Total				72

2.2.2 Sample Preparation

The sample is a beam, as shown in Figure 1. Before casting the concrete, oil was applied to the mould after cleaning it. The moulds were then filled with concrete in layers. The test samples were kept at room temperature for 24 hours, after which they were marked, removed from the moulds, and stored covered in clear freshwater until the test. The test was performed after 28 days because concrete achieves its highest strength after that period of time and its compressive strength indicates its overall strength [66], as shown in Figure 2. This study used four standard concrete mixes and four FRC mixtures. For example, steel fibre-reinforced concrete (SFRC) was utilized to create four concrete mixtures with various seeded crack depths (2 mm, 4 mm, and 6 mm), at a length of 20 mm, and a fibre content of 1% that replaced the cement in the concrete mix. The optimal value of steel fibre used in this study is according to a parametric study for optimizing fibre-reinforced concrete Properties.

Figure-2 Beam sample preparation.

2.2.3 Dynamic Response Testing

The experimental design was similar to approaches used in previous studies [67]. The first seeded crack SFRC sample was set on a Data Physics V55 shaker (Hailsham, UK). The signal generator produced a sine output signal, which sent the signal to the shaker. A mica band heater was used throughout the trials to transmit a temperature load to the samples. An accelerometer was attached to the free end of the beam to monitor the acceleration in real time. The acceleration and time data were recorded on Signal Express software using a DAQ NI 9174 chassis and a DAQ NI 9234 card (Figure 3). The table 3 explains the sensitivity of the used accelerometer in this study

Table 4 explains the sensitivity and reliability of the used accelerometer in this study

Model	Weight gm	Sensitivity mV/g	Range g	Frequency Response Hz (±5%)	Electrical Isolation	Max. Shock gaps	Min. Temp °F (°C)	Max Temp °F (°C)	Environmental Sea	Mounting Method
3055B2	10	100	50	1 to10000	yes	2000	-60(-51)	250(+121)	hermetic	10-32 tapped hole

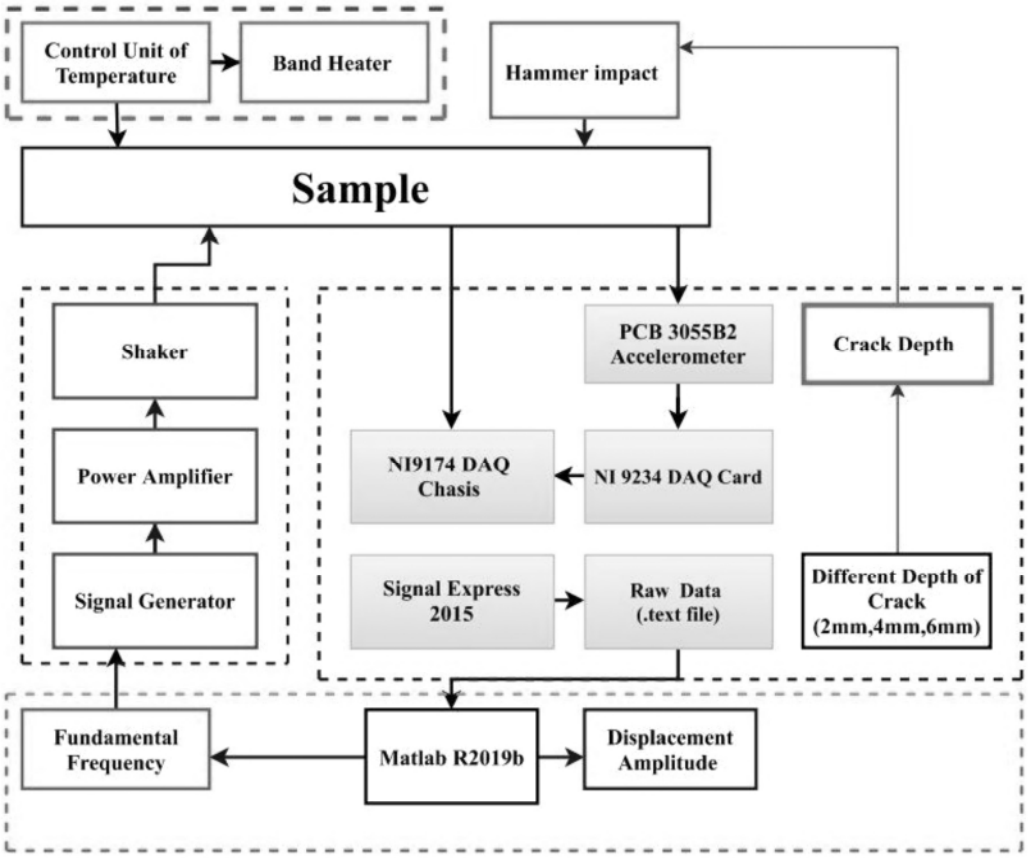

Figure-3 Experimental procedures.

The experiment was performed in stages. First, the fundamental natural frequency of the specimen was determined three times using impact tests. The average number of the frequency response was then calculated. Second, the shaker generated a sinusoidal motion with a displacement amplitude of 1 mm at the measured fundamental frequency. Finally, the shaker powered the beam and vibrated at the frequency, producing the first maximum beam displacement amplitude. The displacement amplitude was calculated and used to investigate the crack. Figure 5 illustrates a seeded crack depth ranging from 2 mm to 6 mm of the CFRC beam. Continuous force vibration caused the depth of the crack, reducing the local rigidity of the crack location and modifying the dynamic response characteristics of the entire system. When the displacement amplitude displayed in real time by the Signal Express program was drastically lowered, the experiment was paused. Next, the fundamental frequency of the system was measured and re-entered. As a result, the experiment was re-started. The methods were used for all seeded crack beams. Figure 3 above shows the experimental steps and Figure 4 below presents the experimental setup.

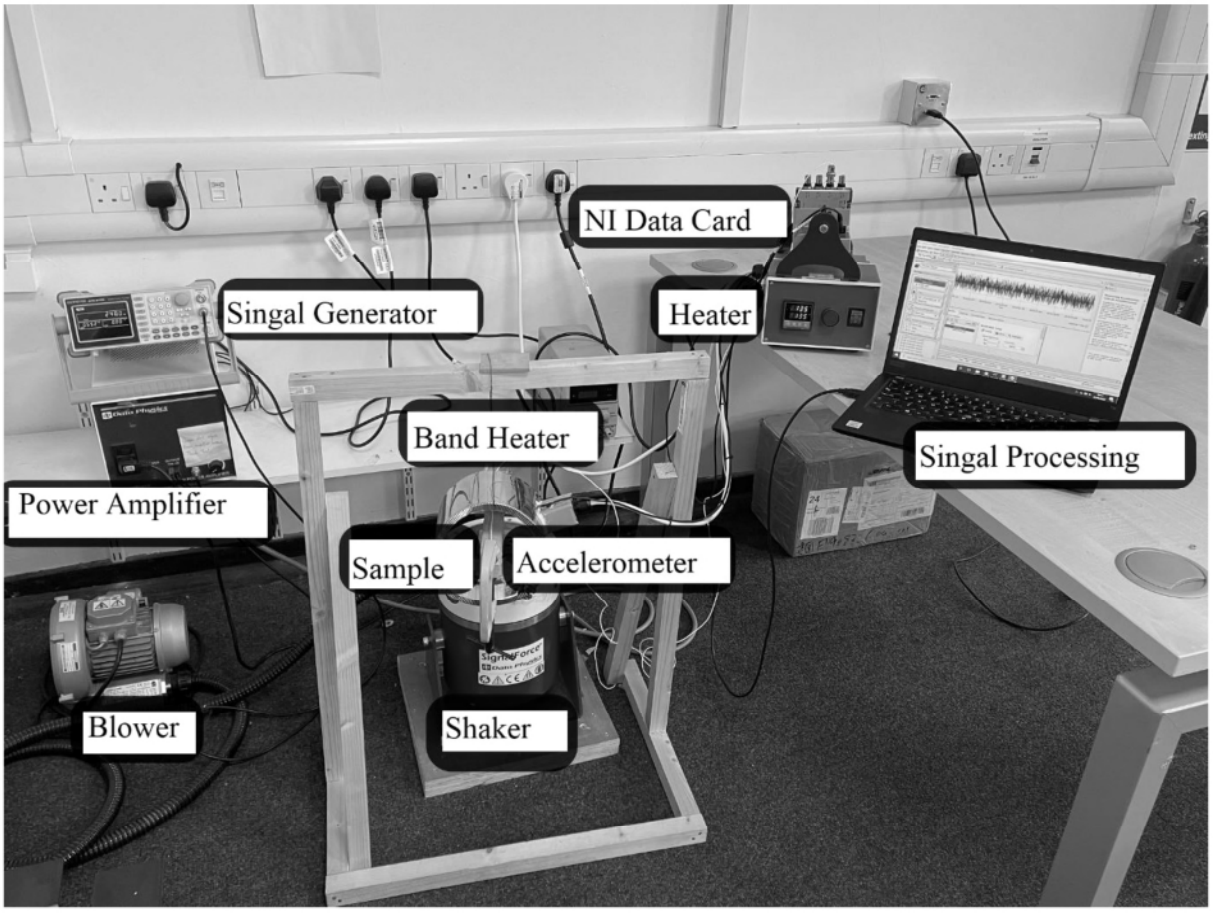

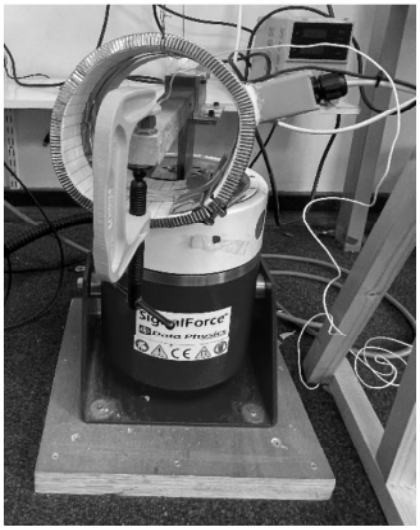

Figure-4 Experimental setup.

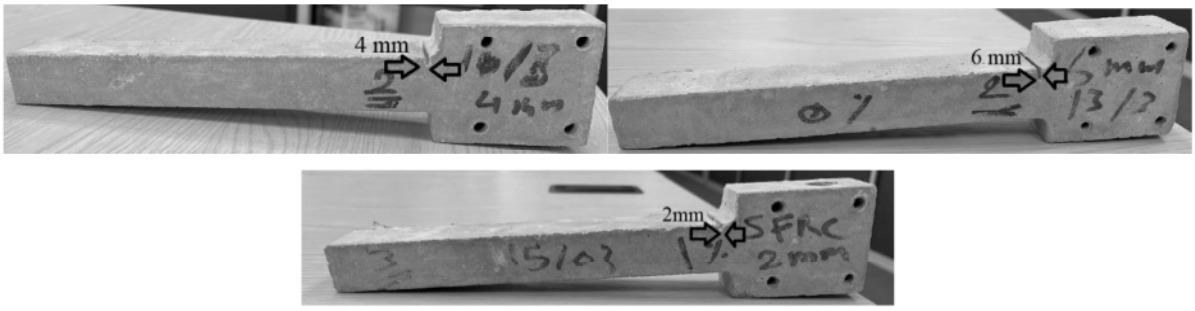

Figure-5 Illustrates a seeded crack depth ranging from 2 mm to 6 mm of an SFRC beam.

2.2.4: Calculation of stress intensity factor

The stress intensity factor is the driving force that drives the crack to grow. This study considers the load applied as the ultimate load (F) at the beam ends to generate the worst deflection situation. The resulting maximum load can be calculated as follows: Max deflection equals the specified amplitude value at resonance. Therefore, Eq (1) amplitude value can be used to determine the load. As a result, the ultimate load at the crack's tip will have a sine wave-like shape with angles between 0 and 360 degrees.

$$\delta_{max} = \frac{PL^3}{3EI} \quad (1)$$

$$\sigma = \frac{M}{Z} \quad (2)$$

Where M is the bending moment, σ Stress at the tip and Z is the section modulus, calculated as

$$Z = \frac{b*h^2}{6} \quad (3)$$

Where b=30 mm and h=25 mm are the cross sections of the cantilever beam in this study.

The minimum and maximum stress values can be provided $\Delta\sigma$ by the load sine graph, which enables it to supply the value needed for ΔK.

$$\Delta K = Y\,\Delta\sigma\,(Pi\ x\ crack\ depth)\ \wedge\ (0.5) \quad (4)$$

From the literature can be calculated Y for mode-1 fracture under bending load specimens. It will be roughly equal to 1.12. Crack depth values are available based on the amplitude value chosen in Eq.1.

3. Analytical Model to Calculate the Natural Frequency during Different Crack Depths

Fundamental frequency, displacement amplitude, and mode shapes are all ways to express a dynamic structural response. This study covers the first two techniques. Ultimately, measuring frequency and structural displacement amplitude is easier and more convenient than monitoring the mode forms in real construction circumstances. The first mode shape is seen in many real structural applications and is primarily responsible for any structural property changes due to its high energy content.

3.1 Abstraction of Good Working Conditions of the Samples in this Study

There are various structures within practical real application scenarios. A cantilevered beam structure was studied in this study because, as with most previous research, a cantilevered beam is an essential element in real engineering applications because it can resist high mechanical loads. Structures such as wings and wind blades may be considered cantilever beams. In addition, the dynamic response of a cantilever beam is more violent when it is excited.

Figure 1 above shows how the cantilever beam in this study was constructed. The beam can be excited by vibrating movement from the fixed left end. To model crack damage in functional structures, the initial seeded crack was on the top surface and close to the stationary end of the beam. There was one crack location. To depict damage in real life, the distance between the beam's start and the fixed end is 200 mm. Furthermore, an additional mass on the free beam end represents an accelerometer in contrast to a practical application. It clamps a mass of 0.6 g and 670 g, respectively, used in later experiments in the research.

3.2 Modelling Crack Size

Cracks alter the local stiffness of a structure. A large crack depth reduces local stiffness significantly. As illustrated in Figure 6, a crack in a beam can be represented by a torsional spring. Ostachowicz and Krawczuk used Equations (5) and (6) to model the torsion spring stiffness related to an open single-sided crack on a beam[4].

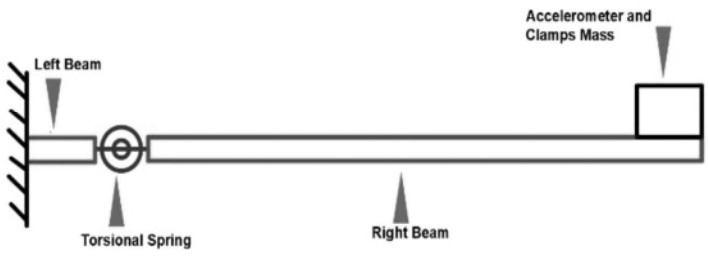

Figure-6 Torsion springs–cantilever beams–accelerometer system.

$$k = \frac{EbH^2}{72\pi f_r\left(\frac{a}{H}\right)} \quad (5)$$

$$f_r\left(\frac{a}{H}\right) = 0.6384\left(\frac{a}{H}\right)^2 - 1.035\left(\frac{a}{H}\right)^3 + 3.7201\left(\frac{a}{H}\right)^4 - 5.1773\left(\frac{a}{H}\right)^5 + 7.553\left(\frac{a}{H}\right)^6 - 7.3324\left(\frac{a}{H}\right)^7 + 2.4909\left(\frac{a}{H}\right)^8 \quad (6)$$

Several previous studies used a similar model of spring stiffness derived from fracture mechanics to study the dynamic behaviour of beam fractures [7–9,11,16,68–70][71][10][72][73].

They employed Equations (5) and (6) directly to investigate the relationship between crack depth and spring stiffness. Their analysis assumed that bending stress was equivalent to stress on the crack upon the beam surface because of the moment constant. The estimated stiffness equations above are, however, only applicable to cracks near the surface. With greater crack propagation depths, this hypothesis may result in spring stiffness inaccuracies. As a result, a mathematical change was introduced into Equation (5), as shown in Equation (7):

$$k = \left(\frac{H-a}{H}\right) \times \frac{E_T bH^2}{72\pi f_r\left(\frac{a}{H}\right)} \quad (7)$$

The additional term $(H - a)/H$ ensures that the stiffness of the spring tends to zero as the crack depth considers the beam thickness, which relates to the actual condition. The contrast between the originally modelled and the modified stiffness is shown in Figure 6. A higher temperature caused a reduction in the elastic modulus, E_T, and, in due course, caused a decrease in natural frequency[74]. Equation (8) introduces E_T, which is a temperature-dependent value in Equation (9).

$$\mathrm{E} = \mathrm{E\_20} * (1.06 - 0.003 * \mathrm{T}) \quad (8)$$

3.3 Natural Frequency of the System

With the revised torsional spring model in Equation (3), a cracked beam is shown as two separate whole beams, as shown in Figure 7 below, consistent with other studies [1–3,5–10,14,16–20,23,24,68,71–73,75–93],Euler-Bernoulli classical beam theory was employed separately for the left and right beams. Thermal expansion owing to thermal loads (high ambient temperature) does not introduce force and timing since the beam has just one fixed end, on the left. The damping effect of the beam is examined because only the basic frequency of the beam is determined. For both beams, the determining variance equation can be written as Equations (9) and (10):

$$E_T I \frac{\partial^4 y_L(x,t)}{\partial x^4} + \rho A \frac{\partial^2 y_L(x,t)}{\partial t^2} = 0 \quad (9)$$

$$E_T I \frac{\partial^4 y_R(x,t)}{\partial x^4} + \rho A \frac{\partial^2 y_R(x,t)}{\partial t^2} = 0 \quad (10)$$

$$I = \frac{bH^3}{12} \qquad A = bH$$

Thermal load variations have an effect on the value of the elastic modulus of the E_T material. The boundary conditions of the two beams can be given as follows:

1. There is no rotation at the fixed end of the beam and, consequently, $\partial y_L(0,t)/\partial x = 0$.
2. There is no displacement at the fixed end of the beam and, consequently, $y_L(0,t) = 0$.
3. Deflection appears at the spring position, hence $y_L(l,t) = y_R(l,t)$.
4. Angular divergence due to spring rotation happens and, consequently, $\partial y_R(l,t)/\partial x - \partial y_L(l,t)/\partial x = (E_T I/k)[\partial^2 y_R(l,t)/\partial x^2]$.
5. The bending moment occurs in the spring position and, therefore, $\partial^2 y_L(l,t)/\partial x^2 = \partial^2 y_R(l,t)/\partial x^2$.
6. Shearing force occurs in the spring position and, therefore, $\partial^3 y_L(l,t)/\partial x^3 = \partial^3 y_R(l,t)/\partial x^3$.
7. There is no bending moment in the free end of the beam and, consequently, $E_T I[\partial^2 y_R(L,t)/\partial x^2] + J_z[\partial^3 y_R(L,t)/\partial t^2 \partial x] = 0$. $J_z$is ignored since it is too small.
8. There is no shearing force at the free tip of the beam and, consequently,

$$E_T I[\partial^3 y_R(L,t)/\partial x^3] - m[\partial^2 y_R(L,t)/\partial t^2] = 0.$$

The overall solution of Equation (9) is

$$y(x,t) = Y(x)\, sin(\omega t) \quad (11)$$

Equation (10) is obtained by substituting Equation (12) into Equation (13):

$$\frac{d^4 Y(x)}{dx^4} - \beta^4 Y(x) = 0 \quad (12)$$

$$\beta^4 = \frac{\omega^2 \rho A}{E_T I}$$

The general solutions of Equation (8) for the left and right beams are presented as Equation (13):

$$Y_L(x) = A_L \sin(\beta x) + B_L \cos(\beta x) + C_L \sinh(\beta x) + D_L \cosh(\beta x)$$

$$Y_R(x) = A_R \sin(\beta x) + B_R \cos(\beta x) + C_R \sinh(\beta x) + D_R \cosh(\beta x) \quad (13)$$

In the boundary conditions, the general solution shown in Equation (13) is used. According to Cramer's rule, the characteristic Equation (10) is produced since at least one constant from A_L to D_R has non-zero solutions.

The equation is used to calculate the value of Equation (14). Next, the different orders of the natural frequencies for the cracked beam with an end mass are computed using Equation (12).

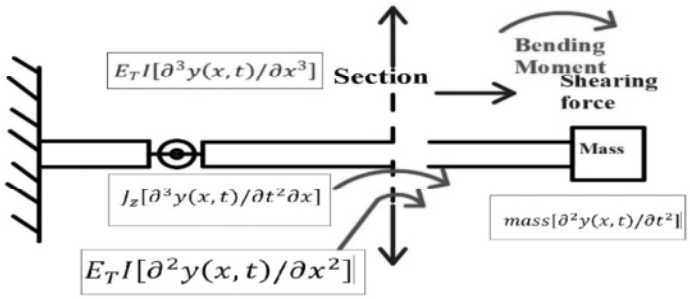

Figure-7 Beam cross-section free body diagram.

$$\begin{vmatrix} 1 & 0 & 1 & 0 & 0 & 0 & 0 & 0 \\ 0 & 1 & 0 & 1 & 0 & 0 & 0 & 0 \\ \sin(\beta l) & \cos(\beta l) & \sinh(\beta l) & \cosh(\beta l) & -\sin(\beta l) & -\cos(\beta l) & -\sinh(\beta l) & -\cosh(\beta l) \\ -\cos(\beta l) & \sin(\beta l) & -\cosh(\beta l) & -\sinh(\beta l) & \cos(\beta l)+\frac{E_T I}{k}\beta\sin(\beta l) & -\sin(\beta l)+\frac{E_T I}{k}\beta\cos(\beta l) & \cosh(\beta l_L)-\frac{E_T I}{k}\beta\sinh(\beta l_L) & \sinh(\beta l_L)-\frac{E_T I}{k}\beta\cosh(\beta l) \\ -\sin(\beta l) & -\cos(\beta l) & \sinh(\beta l) & \cosh(\beta l) & \sin(\beta l) & \cos(\beta l) & -\sinh(\beta l_L) & -\cosh(\beta l) \\ -\cos(\beta l) & \sin(\beta l) & \cosh(\beta l) & \sinh(\beta l) & \cos(\beta l) & -\sin(\beta l) & -\cosh(\beta l) & -\sinh(\beta l) \\ 0 & 0 & 0 & 0 & -\sin(\beta L) & -\cos(\beta L) & \sinh(\beta L) & \cosh(\beta L) \\ 0 & 0 & 0 & 0 & -\cos(\beta L)+\frac{m_{acc}\beta}{\rho A}\sin(\beta L) & \sin(\beta L)+\frac{m_{acc}\beta}{\rho A}\cos(\beta L) & \cosh(\beta L)+\frac{m_{acc}\beta}{\rho A}\sinh(\beta L) & \sinh(\beta L)+\frac{m_{acc}\beta}{\rho A}\cosh(\beta L) \end{vmatrix} = 0 \tag{7}$$

4. Results and Discussion

4.1 Cantilever Beam End Mass System Dynamic Response

Section 2.2.3 describes the fatigue tests on beams with various crack depths and temperatures. The original and adjusted stiffness values were used to create dynamic response models. The analytical model used Equation (8) to calculate the elastic modulus values at various temperatures. Figures 8 and 9 below show the beam's fundamental frequency of the control concrete and the SFRC at the beam tip; the experimental displacement amplitudes of the standard concrete and SFRC are shown in Figures 10 and 11 for the various crack depths. The maximum number of intervals in MATLAB R2019b was surpassed by 2.7 mm when the crack depth was measured at the 5 mm crack location, resulting in approximations that fell short of the desired level of accuracy. The fitted curves for the fundamental frequency were plotted based on the analytical results for crack depths ranging from 0 to 6 mm. The dynamic responses and crack patterns for SFRC concrete slabs and beams derived from the present nonlinear finite element analysis are consistent with those discovered by previous experimental methods[94].

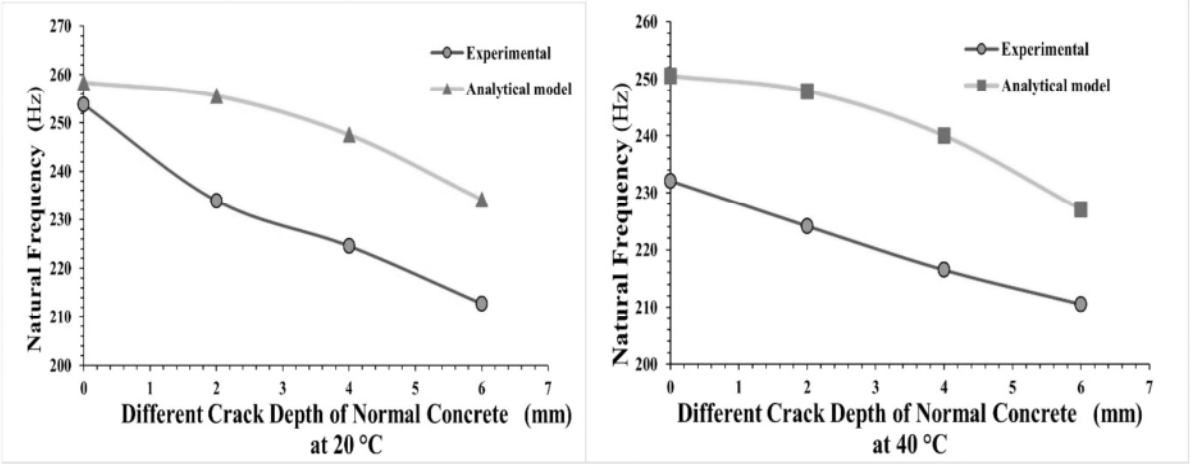

(a) (b)

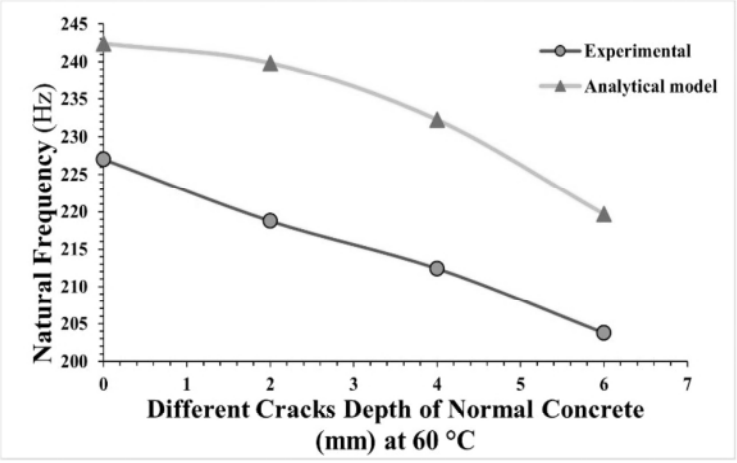

(c)

Figure-8 Natural frequency of normal concrete measured experimentally and predicted using an analytical model at various crack depths and temperatures.

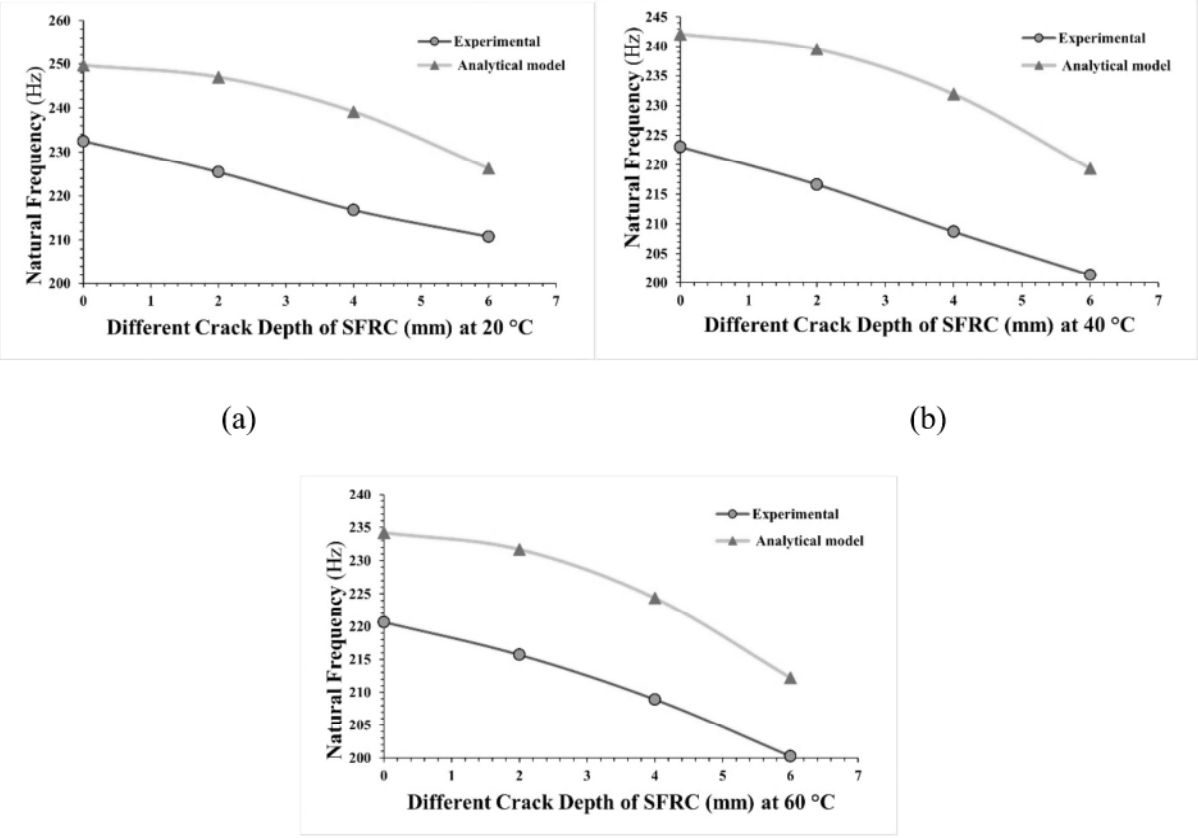

Figure-9 Natural frequency of SFRC measured experimentally and predicted using an analytical model at various crack depths and temperatures.

4.2 Fundamental Frequency of the Seeded Crack Beams

4.2.1 Influence of Crack Depth on the Fundamental Frequency of Normal Concrete and SFRC

Figures 8 and 9 show the results of the impact of crack depth on the natural frequency of cantilever concrete beams with and without steel fibres. Natural frequency and dynamic characteristics are among the essential aspects of construction and are frequently employed, such as for the long-term assessment of bridges over their service life. The relationship between crack depth and a change in fundamental frequency at an ambient temperature of 40 °C at a 5 mm crack location was considered for analysis because the analytical model and experimental data show similar trends for a change in fundamental frequency with crack depth at ambient temperature. There is a gradual decrease in the frequency of samples with differences in crack depth. The experimental results indicated a 7.84% decrease in frequency when the crack depth in the standard concrete was 2 mm. In addition, the results indicate that

the natural frequency of SFRC decreased by about 9% when the steel fibre was added to the concrete beam at the same crack depth. The results showed a slight decrease in the natural frequency of ordinary concrete from 0 mm (253.776 Hz) to 6 mm (212.702) cracking of the beam, about 16.174%. However, the frequency of the SFRC beam gradually decreased to about 9.35%. As a result, the frequencies of the standard concrete and the SFRC were shown to decrease when the crack depths increased. The reduction in natural frequency values observed for the beam's containing fibre was less due to their being induced by a seeded crack, compared with the control reinforced concrete (RC) beam. Furthermore, the Khan model of RC beams reinforced with steel fibres Khan-He has completed the beams' uncracked and cracked beam conditions.

Crack depths are shown in Figure 8 by plotting the fundamental frequency and drop percentage change as predicted by the Khan-He model and data from the experiments. The experimental data and analytical model (see Figures 8 and 9) show that the fundamental frequencies of the normal concrete and the SFRC decrease as the crack depth increase. The fundamental frequency of the control concrete lowers from around 212.72 Hz to 203.7 Hz at a crack depth of 6 mm compared to an entire 25 mm-thick beam, which is just 4.2% of the initial fundamental frequency. Analytical models show that the local drop-in stiffness owing to increased crack depth reduces the stiffness matrix, resulting in a gradual fall in the fundamental frequency.

Notably, the fundamental frequency change is minimal when there is no crack on the surface of the beam. However, when the crack depth of the beam increases, the fundamental frequency decreases. For example, when a 4 mm (one-sixth of the beam thickness) crack is present in the ordinary concrete beam, the frequency decreases by approximately 16 Hz (7% relative change); in contrast, the frequency decreases by around 14 Hz (6% relative change) from the 4 mm crack depth of the FRC beam. In other words, sensitive sensors are necessary when employing crack depth to forecast fundamental frequency.

In general, SFRC frequency is lower than that of conventional concrete. Furthermore, fibre has a negative effect on frequency. As indicated by the data, when the crack depth increases, the frequency decreases. Cracks affect the fatigue lives and limits of concrete and SFRC beams. Thus, crack depth would degrade the fatigue behaviour of the reinforced beams.

4.2.2 Influence of Temperature on the Fundamental Frequency of Normal Concrete and SFRC

Figures 8 and 9 demonstrate the impact of temperature on the natural frequency of cantilever concrete beams with and without steel fibres. There is a gradual decrease in the frequency of the samples with differences in crack depth. The experimental results indicated a 7.84% decrease in frequency when the temperature of the standard concrete was 40 °C. In addition, the results suggest that the natural frequency of SFRC decreased by about 9% when the steel fibre was added to the concrete beam at the same temperature. The results showed a slight decrease in the natural frequency of ordinary concrete

without cracks from 20 °C (253.776 Hz) to 60 °C (226.9 Hz) in the beam (about 10.5%). However, the frequency of the SFRC beam without cracking gradually decreased from 20 °C (232.5 Hz) to 60 °C (220.65 Hz) (about 5.08%). This indicates that the frequency of the standard concrete and the SFRC decreased when the temperature increased. According to previous findings, it is widely accepted that the concrete elastic modulus, geometrical features, constraints, and boundary conditions of construction applications are changed by temperature, which causes variations in fundamental frequencies.

Various studies show that temperature is the most significant environmental element influencing structural vibration [95,96], and that its influence may be higher than that of structural damage [97]. Xia et al. examined the change of modal frequencies against non-uniform temperature distribution for an RC slab by considering the correlations between natural frequencies and temperature. It was amply demonstrated that when temperature increased, natural frequencies decreased [98]. Li et al. found that high temperatures reduced SFRC elastic modulus while increasing its critical strain, and that peak toughness increased initially and then decreased as the temperature rose [99]. The highest value was observed in the frequency of standard concrete at 20 °C. This is related to plasticity formation at lower temperatures and ductility at higher temperatures. When the modal variability generated by daily temperature differences and seasonal temperature fluctuations are coupled, it has a complex influence on structural applications such as bridge construction, dams, and highways. Furthermore, the temperature in the SFRC reached 60 °C at the same time, which is the temperature that causes stiffness reduction. As a result, the change in displacement slop observed after approximately 30 min of heating is also related to the greater deformability of an unreinforced beam at ambient temperature. The frequency of concrete was decreased for two reasons. The first was due to the increase in the temperature, and the second is that the elastic modulus of concrete is slightly impacted by the 1% volume fractions of steel fibres used in this study. However, the elastic modulus of SFRC is anticipated to decrease as more fibres are added. In addition, it is seen that the natural frequency of fibre decreases as the fibre volume fraction increases, which other researchers have demonstrated [100].

In general, SFRC frequency is lower than that of conventional concrete. Furthermore, fibre has a negative effect on frequency. When the temperature increases, as indicated by the data, a decrease in frequency is revealed. Temperature affects the fatigue lives and limits of concrete and SFRC beams. Therefore, high temperature environments would degrade the fatigue behaviour of reinforced beams.

4.3 Influence of Crack Depth on Displacement Amplitude

The displacement amplitude of beams with fibre and without fibre at 0.0 mm, 2 mm, 4 mm, and 6 mm crack depths at different temperatures was examined in order to compare the trends of the displacement amplitude of the samples at the three crack depths. Figures 10 and 11 show the variation in displacement amplitude of the control and SFRC beams with different crack depths. At crack depths of an ordinary concrete beam of 0 mm to 6 mm, the displacement amplitude drops from roughly 0.0034 mm. Similarly,

the drop for the reinforced concrete was from 0 mm to 6 mm; about 0.0042. However, the displacement of the SFRC was higher than that of the standard concrete. For example, at crack depths of 2 mm, 4 mm, and 6 mm, the displacement of the ordinary concrete and the SFRC at 40 °C was (0.0132, 0.0124, 0.0117, 0.0104 mm) and (0.0140, 0.0136, 0.0125, 0.0105 mm), respectively. Moreover, the change in displacement amplitude is as gradual as the crack depth at the top surface of the beam. When the crack depth of the beam is 6 mm, the displacement amplitude falls sharply.

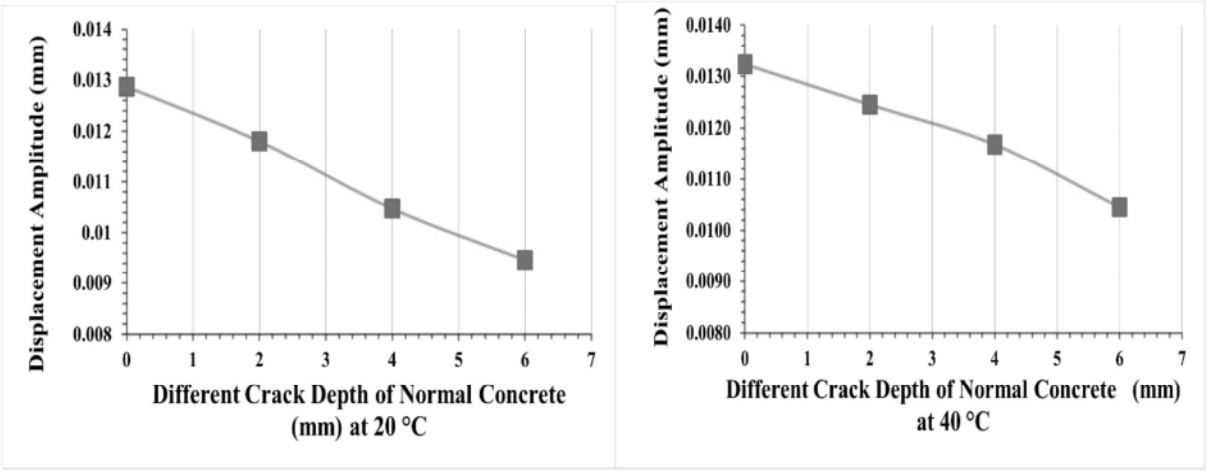

(a) (b)

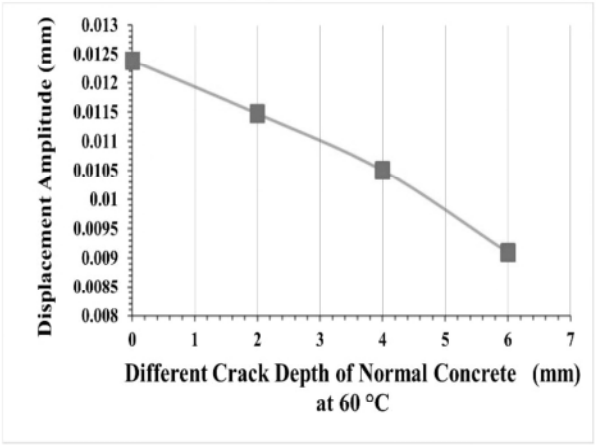

(c)

Figure-10 Displacement amplitudes of normal concrete measured experimentally at various crack depths and temperatures.

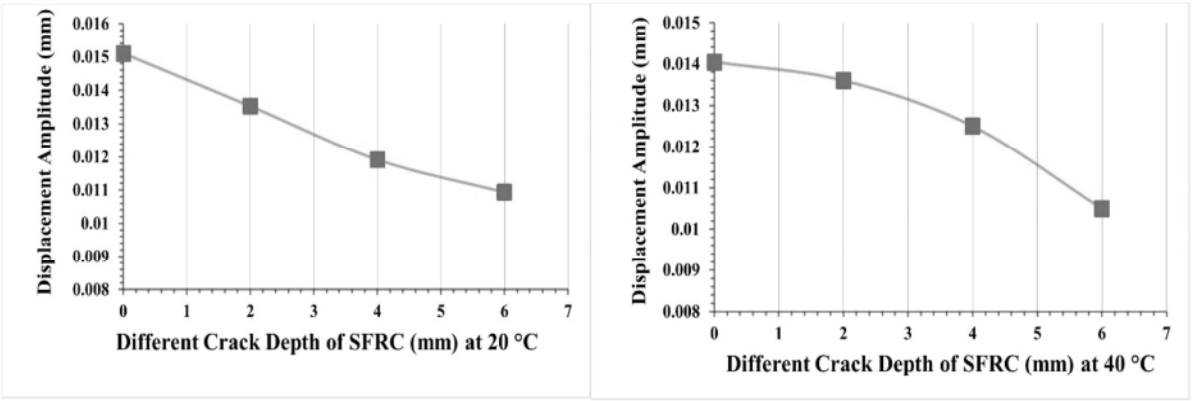

(a) (b)

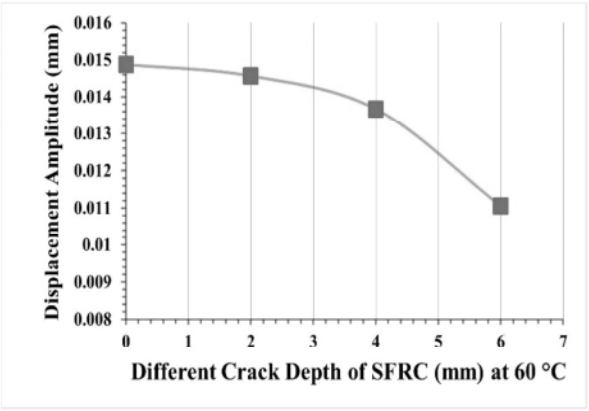

(c)

Figure-11 Displacement amplitudes of SFCR measured experimentally at various crack depths and temperatures.

The decrease in beam displacement amplitude with an increase in crack depth can be ascribed to two factors. First, as the fracture depths increase, the load required to maintain the displacement amplitude of FRC steadily reduces. In other words, the force pushing on the beam reduces gradually. Reduced stress leads to smaller displacement amplitudes. Second, an increasing crack depth enhances beam damping. As a result, the energy released by damping during vibration increases, whereas the displacement amplitude decreases. Previous study support that by using fiber, such as ABS or Polylactic Acid (PLA), in concrete beams increased their ductility but decreased their compressive strength[101]. FRP composites' fatigue resistance was greater than that of other construction materials [102,103]. Matsumoto used a fracture mechanics-based model to evaluate the influence of FRC on fatigue life and discovered that FRC enhances fatigue life [104]. The use of SFRC considerably increased the strength and fatigue life of the concrete by eliminating the open crack region [105].

In general, SFRC displacement is more than that of conventional concrete. Furthermore, fibre has a positive effect on displacement. When a crack increases, as indicated by the data, a decrease in displacement is revealed. Crack depths affect the fatigue lives and limits of concrete and SFRC beams. Therefore, increasing cracks would degrade the fatigue behaviour of the reinforced beams.

4.4 Influence of Temperature on Displacement Amplitude

Figures 10 and 11 show how temperature affected the displacement amplitude of beams with and without steel fibre. The impact of various temperatures on the displacement amplitude of cracked beams is complex, in contrast to all prior response trends. The displacement amplitude of a beam from an intact to a cracked condition is at its lowest at 20 °C, as indicated in Figure 10. At 20 °C, the entire beam has the maximum displacement amplitude but, when the temperature increases, the displacement decreases. The displacement of the SFRC beam was higher than that of the beam without fibre. For example, the displacement of different beams with and without fibre at different crack depths (2 mm, 4 mm, 6 mm) at the same temperature of 40 °C was (0.01245, 0.0117, 0.0104) and (0.0136, 0.0125, 0.0105), respectively. This incidental phenomenon supports the experimental findings of earlier studies [1]. Greater seasonal temperature variations than a dam has previously experienced appear to be more likely to affect its concrete temperature and relative displacement [106]. These phenomena are explained explicitly by the interaction of temperature-dependent excitation loads and variable elastic moduli. When the temperature increases and the beam is exposed to the same external excitation, the overall flexibility of the beam naturally decreases, and the displacement amplitude gradually increases. However, the fundamental frequency decreases in relation to the temperature increase. As a result, the external forces imposed on the beam reduce the displacement amplitude and frequency, lowering the beam displacement amplitude. The overall response of the displacement amplitude of the beam loses monotonicity and becomes more complex because of these two conflicting impacts.

The outcomes above demonstrate a favourable impact of steel fibre particles when applied to dynamic loading, including displacement with exposure to various temperatures (20, 40, 60 °C). Steel softens and eventually decomposes at different temperatures, so the enhanced effect of SFRC on frequency diminishes after it undergoes a high-temperature treatment.

In general, the displacement of plain and FRC decreases with an increase in concrete temperatures. SFRC displacement is more than that of conventional concrete. Furthermore, fibre has a positive effect on displacement. When the temperature increases, as indicated by the data, a decrease in displacement is revealed. Temperatures affect the fatigue lives and limits of concrete and SFRC beams. Therefore, increasing temperatures would degrade the fatigue behaviour of the reinforced beams. As a result, the thermal impacts must be considered when designing concrete structures for safety.

4.5 Calculation of stress intensity factor and crack resistance

Structural behaviour against crack propagation is quite significant for concrete applications. The stress intensity factor represents the crack resistance and fracture toughness of a material [61,62]. Some researchers said that the interaction between the SIFs at the crack's tip symbolizes the conflict between the forces working to open and close the crack: the cohesive force and the crack driving force. Therefore, the concrete's crack resistance qualities should be considered when determining the

equilibrium condition of the SIFs at the crack tip [107,108]. Researchers previously assessed the stress state of reinforced concrete beams with newly formed cracks. The external moment value for beams with an initial fracture is identified, and the crack length lengthens above that value[109,110]. In this study, the stress intensity factor of beams with and without fibre at 2 mm, 4 mm, and 6 mm crack depths at different temperatures was calculated. Figures 12 shows the stress intensity factor variation of the control and SFRC beams with different crack depths. At crack depths of an ordinary concrete beam of 0 mm to 6 mm, the crack resistance was lower than SFRC at 20°C ,40°C, and 60°C. For example, at crack depths of 2 mm, 4 mm, and 6 mm, the crack resistance of the ordinary concrete and the SFRC at 40 °C was (0.344,0.422,0.463) MPa $m^{-1/2}$ and (0.386,0.546,0.536) MPa $m^{-1/2}$, respectively. Moreover, the change in resistance is as gradual as the crack depth at the top surface of the beam. These observations are comparable with previous research where fibre impacts on concrete toughness were found more significant in the tearing mode than in the tension mode.

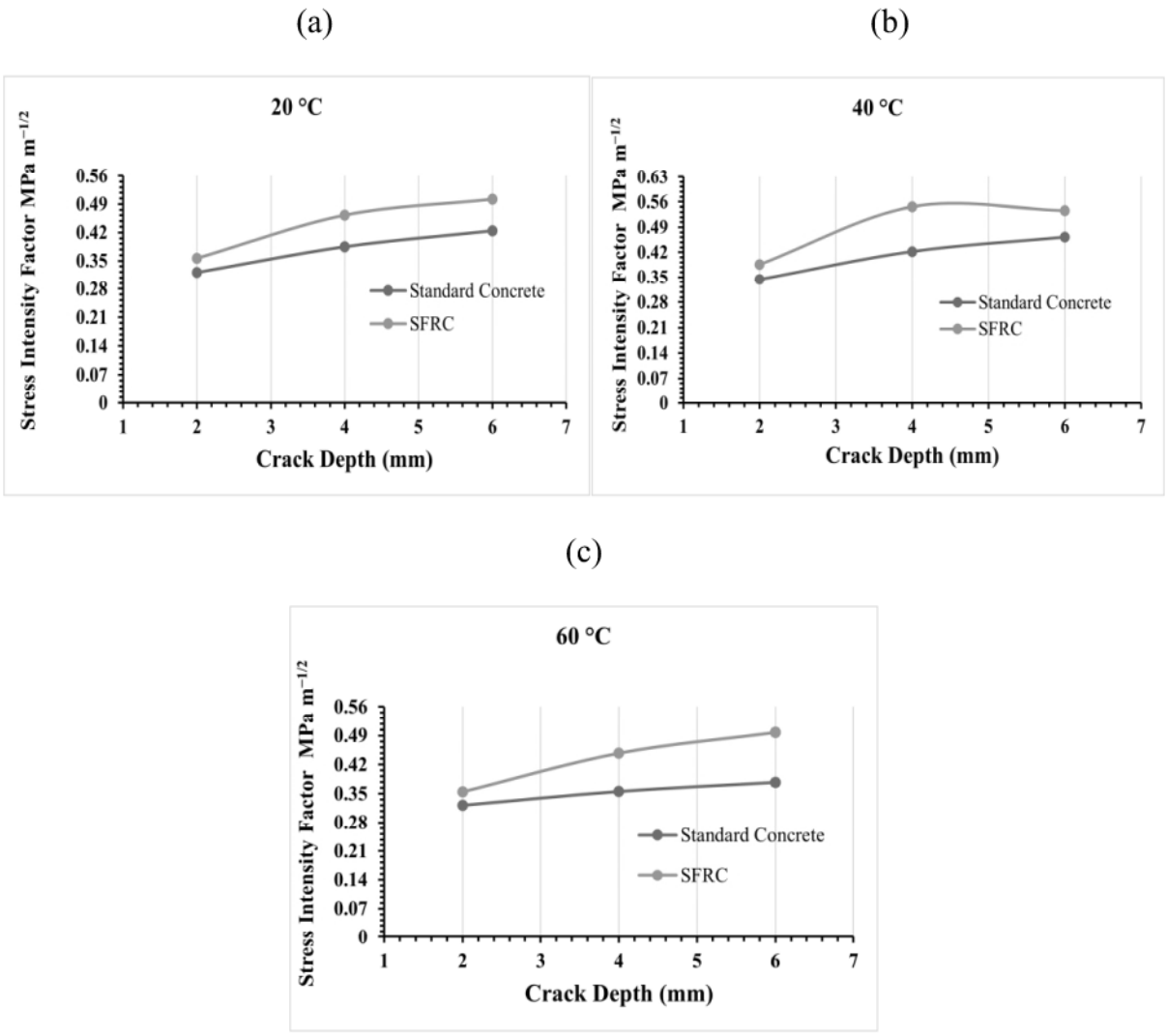

Figure-12 Concrete stress intensity factor with and without steel fibre at various crack depths (mm) and temperatures.

In general, the SIF of plain concrete decreases with increased concrete temperatures. However, there is no temperature impact on the SIF of steel fibre-reinforced concrete beam. In addition, it was observed that the SIF of a concrete beam with reinforcement reduces as crack length increases. As a result, unstable crack propagation lowers its load-carrying capacity but does not result in the beam being destroyed quickly[110].

4.6 Statistical validation of results

The SPSS software was used to perform Statistical validation on the experimental data. The Pearson correlation method was used to describe the relationship between the obtained values of stress intensity factor against the input values of temperature, and crack depth. Tables 5,6,7 and 8 summarize the findings using the correlation and other descriptive statistics of the results for both the standard concrete and the SFRC, respectively. The statistical details indicate that the biserial correlation between the stress intensity factor and the crack depth has two asterisks, which means this correlation is significant at 0.05 level (2-tailed) [111]. The stress intensity factor and crack depth are closely correlated with the correlation numbers equal to 0.826 and 0.948 for normal concrete and SFRC respectively. The estimated p-value was less than 0.001, which means that there is a strong relationship in between the obtained results of stress intensity factor and the input variable i.e., crack depth. However, the estimated p-value was more than 0.05, about 0.140 and 0.106, which means there is a less relationship between the obtained results of the stress intensity factor and the input variable i.e., temperatures for standard concrete and SFRC, respectively.

Table 5 shows the statistical Correlation of normal concrete between SIF, Temperatures, and Crack depths

Correlations				
Crack Depths (mm)		Crack Depths (mm)	SIF	Temperatures (°C)
	Pearson Correlation	1	.826**	0
	Sig. (2-tailed)		<0.001	1
	N	27	27	27
SIF	Pearson Correlation	.826**	1	0.140
	Sig. (2-tailed)	,<0.001		0.487
	N	27	27	27
Temperatures (°C)	Pearson Correlation	0	0.140	1
	Sig. (2-tailed)	1	0.487	

	N	27	27	27
** Correlation is significant at the 0.05 level (2-tailed).				

Table 6 the Descriptive Statistics of normal concrete results

Descriptive Statistics			
	Mean	Std. Deviation	N
CRACK	4	1.66410059	27
SIF	0.361462	0.08151676	27
TEM	40	16.64100589	27

Table 7 shows the statistical Correlation of SFRC between SIF, Temperatures, and Crack depths

Correlations				
		Crack Depths (mm)	SIF	Temperatures (°C)
Crack Depths (mm)	Pearson Correlation	1	.948**	0
	Sig. (2-tailed)		<.001	1
	Sum of Squares and Cross-products	72	3.615	0
	Covariance	2.769	0.139	0
	N	27	27	27
SIF	Pearson Correlation	.948**	1	0.106
	Sig. (2-tailed)	<.001		0.6
	Sum of Squares and Cross-products	3.615	0.202	4.029
	Covariance	0.139	0.008	0.155
	N	27	27	27
Temperatures (°C)	Pearson Correlation	0	0.106	1
	Sig. (2-tailed)	1	0.6	
	Sum of Squares and Cross-products	0	4.029	7200
	Covariance	0	0.155	276.923
	N	27	27	27
** Correlation is significant at the 0.05 level (2-tailed).				

Based on the p-values in the preceding tables, we can confirm that an increase the crack depth has the highest statistical impact on crack resistance of both SFRC and normal concrete. Temperature has a less impact on crack resistance for SFRC and normal concrete. Tables 6 and 8 provides statistical information regarding the impact of crack depths and temperatures. The mean data for all the specimens

was calculated at different temperatures (20,40,60) °C and different crack depths(2mm,4mm,6mm). The statistical analysis of the normal concrete samples was also based on the same method.

Table 8 the Descriptive Statistics of SFRC results

Descriptive Statistics			
	Mean	Std. Deviation	N
Crack Depths (mm)	4	1.6641	27
Stress intensity factor	0.3857772	0.088176	27
Temperature(°C)	40	16.641	27

4.7 Comparison and Evaluation of Fundamental Frequency Variations

Experimental data and analytical model outputs of the fundamental frequencies of standard concrete and SFRC for different crack depths and temperatures are shown in Figures 8 and 9. The fundamental frequency of the specimens decreases as the seeded crack depth increases, according to the experimental results and the calculations of the analytical model. A similar result was found previously [1]. The fundamental frequencies of standard concrete and SFRC were determined using an identical model, as shown by a comparison of the results of the analytical model-based fundamental frequency calculations. The basic frequency curve of the original spring stiffness model tends to decrease as the crack depth increases. In contrast, the modified spring stiffness model drops rapidly and decreases even more rapidly as the crack depth increases. At a temperature of 60 °C of the concrete without steel fibres, the fundamental frequency results of the experimental and modelling results were 227 Hz at zero depth, 218.726 Hz at 2 mm, and 203.8 Hz at 6 mm. This is due to increases in the seeded crack depth and the temperature rises. From 0 to 6 mm fracture depth, the results of the experiment show a slight increase from 6.4 to 7.23% in terms of percentage proportion to the original stiffness model.

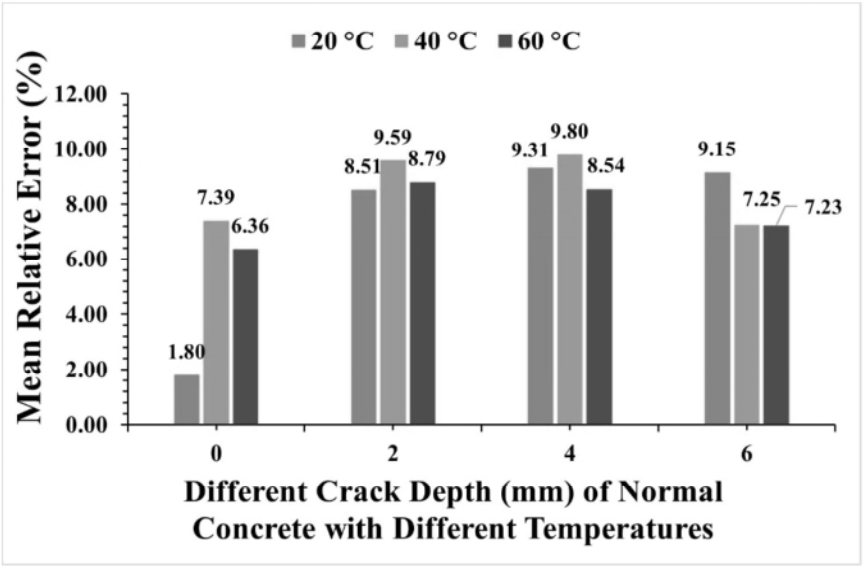

Figure-13 Relative variance between the analytical model and experiment results of normal concrete.

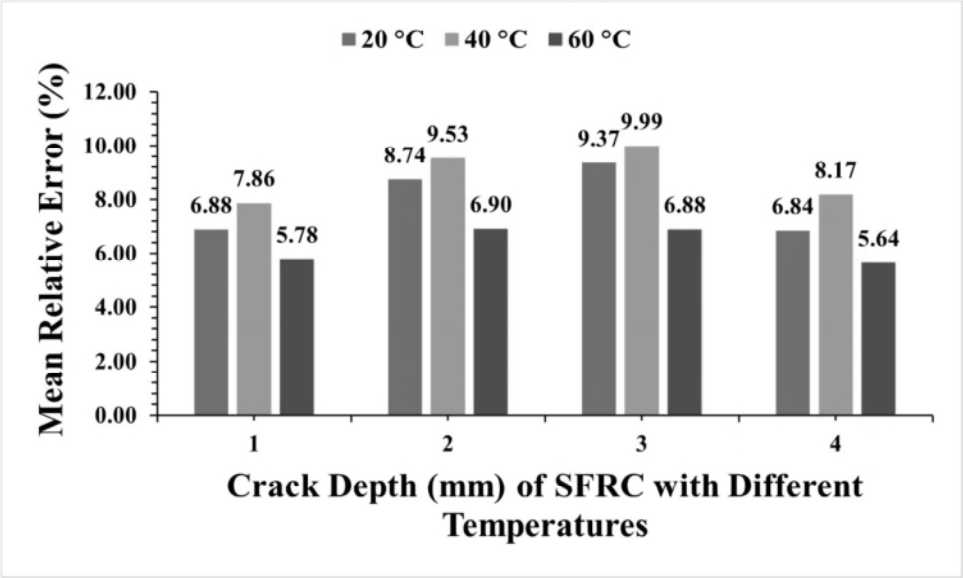

Figure-14 Relative variance between the analytical model and experiment results of SFRC.

Section 3.2 reported the spring model of crack depth and the difference in the fundamental frequency of crack depths. It was originally assumed that the stress field and surface stresses of bending beam cracks were of equal size in the spring stiffness modelling process. It is only possible to use this estimate for shallow cracks near the surface of a beam. Stress errors increase as the crack depth increases. There are two different terms in the suggested Khan-He model that ensure that the stiffness coefficient of the spring is zero when a beam is cracked. When comparing the results of the analytical model with the experimental data, it becomes clear that the model's projected values, particularly at high crack depths, can be accepted. As shown in Figures 8 and 9, the experimental data and the spring stiffness model have significant disparities. Temperatures and crack depths have varying fundamental frequencies. Furthermore, the variation in the fundamental frequency with crack depth is consistent across all plots.

A crack depth at 2 mm under 40 °C at the 5 mm crack position is shown. There are signs of good argument between the results of the different crack depth tests, which are summarised here. Figures 13 and 14 depict the differences between the analytical and experimental findings produced using the analytical model, as shown by the relative difference. The fundamental frequencies computed using the Khan-He Model and the experimental results for different fracture depths grow increasingly dissimilar as the crack depth increases. When crack depths ranging from 2 mm to 6 mm are applied, the Khan-He model produces fundamental frequencies within 10% of the experimental data. Compared to crack depths of 2 mm and 6 mm, the variation in fundamental frequency is just 8.74% and 5.64%, respectively. The fundamental frequency of the analytical model was determined using a second-order polynomial fit because the precision of the MATLAB approach was insufficient. The use of this fit likely contributed to the 10% disparity between the value and the experimental data.

There are signs of good arguments between the results of the different crack depth tests, which are summarised here. Figures 13 and 14 depict the difference between the analytical and experimental findings produced using the analytical model, as shown by the relative difference. The fundamental frequencies computed using the Khan-He Model and the experimental results for different fracture depths become increasingly dissimilar as the crack depth increases. When crack depths ranging from 2 mm to 6 mm are applied, the Khan-He model produces fundamental frequencies within 10% of the experimental data. Compared to crack depths of 2 mm and 6 mm of SFRC, the variation in fundamental frequency is just 0.08% and 0.07%, respectively. The analytical model fundamental frequency was determined using a second-order polynomial fit because the precision of the MATLAB approach was insufficient. The use of this fit likely contributed to the 10% disparity between the value and the experimental data.

In general, the values of the fundamental frequencies predicted by the Khan-He model matched those observed in the experiments. The fundamental frequency response of the beam may be accurately estimated for specified crack depths, compared to the experimental results.

5.Conclusion

In this paper, the efficacy of FRC beams for fracture resistance is investigated under coupled loads, i.e., dynamic load at relatively high temperatures. Cantilever FRC beams are subjected to bending loads at various temperature levels using a modal exciter in a band heater. The variation in the dynamic response parameters of the beam, such as modal amplitude and frequency, is examined and compared to experimental data for regular and reinforced concrete beams. The findings of this investigation are as follows:

- The results showed a slight decrease in the natural frequency of ordinary concrete from 0 mm (253.776 Hz) to 6 mm (212.702) cracking of the beam, about 16.174%. However, the frequency

of the SFRC beam gradually decreased to about 9.35%. As a result, the frequencies of the standard concrete and the SFRC decreased when the crack depths increased.

- In the present study, the temperature affected the natural frequency of both the unreinforced and the FRC. The findings show that the natural frequency of SFRC samples was lower than the typical frequency of concrete. Furthermore, the results showed a slight decrease in the natural frequency of ordinary concrete without cracks from 20 °C (253.776 Hz) to 60 °C (226.9 Hz) in the beam (about 10.5%). However, the frequency of the SFRC beam without cracking decreased gradually from 20 °C (232.5 Hz) to 60 °C (220.65 Hz) (about 5.08%). As a result, the frequency of the standard concrete and the SFRC decreased when the temperature increased
- Temperatures affect the fatigue life of concrete and SFRC beams. Therefore, increasing temperatures would degrade the fatigue behaviour of the reinforced beams.

- The displacement of the SFRC was higher than that of the standard concrete. For example, at crack depths of 2 mm, 4 mm, and 6 mm, the displacement of the ordinary concrete and the SFRC at 40 °C was (0.0132, 0.0124, 0.0117, 0.0104 mm) and (0.0140, 0.0136, 0.0125, 0.0105 mm), respectively. Moreover, the change in displacement amplitude is as gradual as the crack depth at the top surface of the beam. When the crack depth of the beam is 6 mm, the displacement amplitude falls sharply.

- The displacement of the SFRC beam was higher than that of the beam without fibre. For example, the displacement of different beams with and without fibre at different crack depths (2 mm, 4 mm, 6 mm) at the same temperature of 40 °C was (0.01245, 0.0117, 0.0104) and (0.0136, 0.0125, 0.0105) respectively. As a result, fibre has a positive effect on displacement.

- The values of the fundamental frequencies predicted by the Khan-He model matched those observed in the experiments. The fundamental frequency response of the beam may be accurately estimated for specified crack depths compared to the experimental results. When crack depths ranging from 2 mm to 6 mm were applied, the Khan-He model produced fundamental frequencies within 10% of the experimental data. Compared to crack depths of 2 mm and 6 mm of SFRC, the variation in fundamental frequency is just 0.08% and 0.07%, respectively.
- The SIF and displacement amplitude characteristics show that steel fibre-reinforced concrete specimens have excellent ductile behaviour and crack resistance compared to ordinary concrete samples. The SIF of plain concrete decreases with increased concrete temperatures. However, there is no significant temperature impact on the SIF of steel fibre-reinforced concrete beams.

- Based on the p-values in the tables 5,6,7 and 8, we can confirm that an increase the crack depth has the highest statistical impact on crack resistance of both SFRC and normal concrete. Temperature has a less impact on crack resistance for SFRC and normal concrete.

References

[1] B.A. Zai, A. Mujtaba, M. Shahzad, A. Mansoor, A.N. Saquib, K.A. Khan, M. Asif, S.Z. Khan, M.A. Khan, Prediction of crack depth and fatigue life of an acrylonitrile butadiene styrene cantilever beam using dynamic response, ASTM International, 2020.

[2] B.A. Zai, M.A. Khan, K.A. Khan, A. Mansoor, A novel approach for damage quantification using the dynamic response of a metallic beam under thermo-mechanical loads, J. Sound Vib. 469 (2020) 115134.

[3] H. Baqasah, F. He, B.A. Zai, M. Asif, K.A. Khan, V.K. Thakur, M.A. Khan, In-situ dynamic response measurement for damage quantification of 3D printed ABS cantilever beam under thermomechanical load, Polymers (Basel). 11 (2019) 2079.

[4] W.M. Ostachowicz, M. Krawczuk, Analysis of the effect of cracks on the natural frequencies of a cantilever beam, J. Sound Vib. 150 (1991) 191–201.

[5] K. Zhang, X. Yan, Multi-cracks identification method for cantilever beam structure with variable cross-sections based on measured natural frequency changes, J. Sound Vib. 387 (2017) 53–65.

[6] A.C. Altunışık, F.Y. Okur, V. Kahya, Modal parameter identification and vibration based damage detection of a multiple cracked cantilever beam, Eng. Fail. Anal. 79 (2017) 154–170.

[7] B.P. Nandwana, S.K. Maiti, Modelling of vibration of beam in presence of inclined edge or internal crack for its possible detection based on frequency measurements, Eng. Fract. Mech. 58 (1997) 193–205. https://doi.org/10.1016/S0013-7944(97)00078-7.

[8] J. Hu, R.Y. Liang, An integrated approach to detection of cracks using vibration characteristics, J. Franklin Inst. 330 (1993) 841–853. https://doi.org/10.1016/0016-0032(93)90080-E.

[9] H. Nahvi, M. Jabbari, Crack detection in beams using experimental modal data and finite element model, Int. J. Mech. Sci. 47 (2005) 1477–1497. https://doi.org/10.1016/j.ijmecsci.2005.06.008.

[10] K.H. Barad, D.S. Sharma, V. Vyas, Crack detection in cantilever beam by frequency based method, Procedia Eng. 51 (2013) 770–775. https://doi.org/10.1016/j.proeng.2013.01.110.

[11] S. Dastjerdi, M. Abbasi, A vibration analysis of a cracked micro-cantilever in an atomic force microscope by using transfer matrix method, Ultramicroscopy. 196 (2019) 33–39. https://doi.org/10.1016/j.ultramic.2018.09.014.

[12] G.-R. Gillich, N.M.M. Maia, I.-C. Mituletu, Z.-I. Praisach, M. Tufoi, I. Negru, Early structural damage assessment by using an improved frequency evaluation algorithm, Lat. Am. J. Solids Struct. 12 (2015) 2311–2329.

[13] M. Chati, R. Rand, S. Mukherjee, Modal analysis of a cracked beam, J. Sound Vib. 207 (1997) 249–270.

[14] K. Mazanoglu, I. Yesilyurt, M. Sabuncu, Vibration analysis of multiple-cracked non-uniform beams, J. Sound Vib. 320 (2009) 977–989.

[15] G.R. Gillich, Z.I. Praisach, M. Abdel Wahab, H. Furdui, A new modal-based damage location indicator, in: Int. Conf. Noise Vib. Eng., 2014: pp. 499–512.

[16] D.P. Patil, S.K. Maiti, Detection of multiple cracks using frequency measurements, Eng. Fract. Mech. 70 (2003) 1553–1572. https://doi.org/10.1016/S0013-7944(02)00121-2.

[17] N.T. Khiem, H.T. Tran, A procedure for multiple crack identification in beam-like structures from natural vibration mode, J. Vib. Control. 20 (2014) 1417–1427.

[18] P.F. Rizos, N. Aspragathos, A.D. Dimarogonas, Identification of crack location and magnitude in a cantilever beam from the vibration modes, J. Sound Vib. 138 (1990) 381–388.

[19] K.V. Nguyen, Mode shapes analysis of a cracked beam and its application for crack detection, J. Sound Vib. 333 (2014) 848–872.

[20] R. Revi, V.S. Indu, Crack detection of propped cantilever beam using dynamic analysis, Int. J. Tech. Res. Appl. 3 (2015) 2320–8163.

[21] A.K. Pandey, M. Biswas, M.M. Samman, Damage detection from changes in curvature mode shapes, J. Sound Vib. 145 (1991) 321–332.

[22] E. Manoach, J. Warminski, L. Kloda, A. Teter, Numerical and experimental studies on vibration based methods for detection of damage in composite beams, Compos. Struct. 170 (2017) 26–39.

[23] B.A. Zai, M.A. Khan, A. Mansoor, S.Z. Khan, K.A. Khan, Instant dynamic response measurements for crack monitoring in metallic beams, Insight-Non-Destructive Test. Cond. Monit. 61 (2019) 222–229.

[24] M.A. Khan, S.Z. Khan, W. Sohail, H. Khan, M. Sohaib, S. Nisar, Mechanical fatigue in aluminium at elevated temperature and remaining life prediction based on natural frequency evolution, Fatigue Fract. Eng. Mater. Struct. 38 (2015) 897–903.

[25] A. Gupta, N.K. Jain, R. Salhotra, Effect of thermal environment on vibration analysis of isotropic micro plate with inclined crack based on modified couple stress theory, in: 24th Int. Congr. Sound Vib., 2017.

[26] L. Zhao, H. Jin, Effect of temperature on natural frequencies of bridge structure of metallurgical crane, IOP Conf. Ser. Mater. Sci. Eng. 1043 (2021). https://doi.org/10.1088/1757-899X/1043/4/042047.

[27] H. Li, Z. Siqi, X. Shi, H. Wu, Q. Zhaoye, L. Pengxu, X. Wang, G. Zhongwei, Thermal-vibration aging of fiber-reinforced polymer cylindrical shells with polyurea coating: Theoretical and experimental studies, Mech. Adv. Mater. Struct. (2022) 1–16.

[28] M. Ali, A. Liu, H. Sou, N. Chouw, Mechanical and dynamic properties of coconut fibre reinforced concrete, Constr. Build. Mater. 30 (2012) 814–825. https://doi.org/10.1016/j.conbuildmat.2011.12.068.

[29] D. Anastasopoulos, E.P.B. Reynders, S. François, G. De Roeck, G. Van Lysebetten, P. Van Itterbeeck, N. Huybrechts, Vibration-based monitoring of an FRP footbridge with embedded fiber-Bragg gratings: Influence of temperature vs. damage, Compos. Struct. 287 (2022) 115295. https://doi.org/10.1016/j.compstruct.2022.115295.

[30] B. Zima, M. Krajewski, The vibration-based assessment of the influence of elevated temperature on the condition of concrete beams with pultruded GFRP reinforcement, Compos. Struct. 282 (2022) 115040. https://doi.org/10.1016/j.compstruct.2021.115040.

[31] L. Feo, F. Ascione, R. Penna, D. Lau, M. Lamberti, An experimental investigation on freezing and thawing durability of high performance fiber reinforced concrete (HPFRC), Compos. Struct. 234 (2020) 111673. https://doi.org/10.1016/j.compstruct.2019.111673.

[32] A. Zhou, Q. Qiu, C.L. Chow, D. Lau, Interfacial performance of aramid, basalt and carbon fiber reinforced polymer bonded concrete exposed to high temperature, Compos. Part A Appl. Sci. Manuf. 131 (2020) 105802. https://doi.org/10.1016/j.compositesa.2020.105802.

[33] L. Jin, J. Bai, R. Zhang, L. Li, X. Du, Effect of elevated temperature on thelow-velocity impact performances of reinforced concrete slabs, Int. J. Impact Eng. 149 (2021) 103797. https://doi.org/10.1016/j.ijimpeng.2020.103797.

[34] M.B. Bankir, U.K. Sevim, Performance optimization of hybrid fiber concrete according to mechanical properties, Constr. Build. Mater. 261 (2020) 119952.

[35] M. Song, J. Wang, L. Yuan, C. Luan, Z. Zhou, Investigation on crack recovery behavior of engineered cementitious composite (ECC) incorporated memory alloy fiber at low temperature, ES Mater. Manuf. (2022).

[36] M. Ozturk, Embedded smart sensor dipole antennas for real-time damage assessment, humidity, and temperature monitoring in reinforced and non-reinforced concrete structures, Int. J. Microw. Wirel. Technol. 14 (2022) 482–491. https://doi.org/10.1017/S1759078721001409.

[37] J.N. Eiras, T. Kundu, M. Bonilla, J. Payá, Nondestructive monitoring of ageing of alkali resistant glass fiber reinforced cement (GRC), J. Nondestruct. Eval. 32 (2013) 300–314. https://doi.org/10.1007/s10921-013-0183-y.

[38] D. Shen, C. Liu, J. Kang, Q. Yang, M. Li, C. Li, X. Zeng, Early-age autogenous shrinkage and tensile creep of hooked-end steel fiber reinforced concrete with different thermal treatment temperatures, Cem. Concr. Compos. 131 (2022) 104550. https://doi.org/10.1016/j.cemconcomp.2022.104550.

[39] M. Regni, D. Arezzo, S. Carbonari, F. Gara, D. Zonta, Effect of Environmental Conditions on the Modal Response of a 10-Story Reinforced Concrete Tower, Shock Vib. 2018 (2018). https://doi.org/10.1155/2018/9476146.

[40] R. Serafini, S.R.A. Dantas, R.P. Salvador, R.R. Agra, D.A.S. Rambo, A.F. Berto, A.D. de Figueiredo, Influence of fire on temperature gradient and physical-mechanical properties of macro-synthetic fiber reinforced concrete for tunnel linings, Constr. Build. Mater. 214 (2019) 254–268. https://doi.org/10.1016/j.conbuildmat.2019.04.133.

[41] H. Xargay, P. Folino, N. Nuñez, M. Gómez, A. Caggiano, E. Martinelli, Acoustic Emission behavior of thermally damaged Self-Compacting High Strength Fiber Reinforced Concrete, Constr. Build. Mater. 187 (2018) 519–530. https://doi.org/10.1016/j.conbuildmat.2018.07.156.

[42] H.H. Nguyễn, J. Il Choi, K. Il Song, J.K. Song, J. Huh, B.Y. Lee, Self-healing properties of

cement-based and alkali-activated slag-based fiber-reinforced composites, Constr. Build. Mater. 165 (2018) 801–811. https://doi.org/10.1016/j.conbuildmat.2018.01.023.

[43] L. Biolzi, G.L. Guerrini, G. Rosati, Overall structural behavior of high strength concrete specimens, Constr. Build. Mater. 11 (1997) 57–63.

[44] B. Calder, Concrete and Culture: a material history, J. Archit. 18 (2013) 744–756. https://doi.org/10.1080/13602365.2013.841352.

[45] L. Pham, G. Lu, P. Tran, Influences of printing pattern on mechanical performance of three-dimensional-printed fiber-reinforced concrete, 3D Print. Addit. Manuf. 9 (2022) 46–63.

[46] V. Nguyen-Van, P. Tran, C. Peng, L. Pham, G. Zhang, H. Nguyen-Xuan, Bioinspired cellular cementitious structures for prefabricated construction: Hybrid design & performance evaluations, Autom. Constr. 119 (2020) 103324.

[47] N.J. Vickers, Animal communication: when i'm calling you, will you answer too?, Curr. Biol. 27 (2017) R713–R715.

[48] Y. Chen, J.F. Davalos, I. Ray, H.-Y. Kim, Accelerated aging tests for evaluations of durability performance of FRP reinforcing bars for concrete structures, Compos. Struct. 78 (2007) 101–111.

[49] P.N. Balaguru, S.P. Shah, Fiber-reinforced cement composites, 1992.

[50] K.G. Kuder, S.P. Shah, Processing of high-performance fiber-reinforced cement-based composites, Constr. Build. Mater. 24 (2010) 181–186.

[51] S. Banerji, V. Kodur, Effect of temperature on mechanical properties of ultra- high performance concrete, Fire Mater. 46 (2022) 287–301.

[52] I. Lövgren, Fibre-reinforced Concrete for Industrial Construction–a fracture mechanics approach to material testing and structural analysis, Chalmers Tekniska Hogskola (Sweden), 2005.

[53] M. Malik, S.K. Bhattacharyya, S. V Barai, Thermal and mechanical properties of concrete and its constituents at elevated temperatures: A review, Constr. Build. Mater. 270 (2021) 121398.

[54] A. Millard, P. Pimienta, Modelling of Concrete Behaviour at High Temperature, Springer, 2019.

[55] X. Luo, W. Sun, S.Y.N. Chan, Effect of heating and cooling regimes on residual strength and microstructure of normal strength and high-performance concrete, Cem. Concr. Res. 30 (2000) 379–383.

[56] F. Stoll, J.E. Saliba, L.E. Casper, Experimental study of CFRP-prestressed high-strength concrete bridge beams, Compos. Struct. 49 (2000) 191–200.

[57] H.S. Kim, Y.S. Shin, Flexural behavior of reinforced concrete (RC) beams retrofitted with hybrid fiber reinforced polymers (FRPs) under sustaining loads, Compos. Struct. 93 (2011) 802–811.

[58] C. Gong, W. Ding, K.M. Mosalam, S. Günay, K. Soga, Comparison of the structural behavior of reinforced concrete and steel fiber reinforced concrete tunnel segmental joints, Tunn. Undergr. Sp. Technol. 68 (2017) 38–57.

[59] X. Liu, Q. Sun, Y. Yuan, L. Taerwe, Comparison of the structural behavior of reinforced concrete tunnel segments with steel fiber and synthetic fiber addition, Tunn. Undergr. Sp. Technol. 103 (2020) 103506.

[60] L. Li, R. Zhang, L. Jin, X. Du, J. Wu, W. Duan, Experimental study on dynamic compressive

behavior of steel fiber reinforced concrete at elevated temperatures, Constr. Build. Mater. 210 (2019) 673–684.

[61] A. Razmi, M.M. Mirsayar, On the mixed mode I/II fracture properties of jute fiber-reinforced concrete, Constr. Build. Mater. 148 (2017) 512–520.

[62] M. Fakhri, E.H. Kharrazi, M.R.M. Aliha, Mixed mode tensile–In plane shear fracture energy determination for hot mix asphalt mixtures under intermediate temperature conditions, Eng. Fract. Mech. 192 (2018) 98–113.

[63] M. Kosior-Kazberuk, P. Berkowski, Fracture mechanics parameters of fine grained concrete with polypropylene fibres, Procedia Eng. 161 (2016) 157–162.

[64] Z. Wang, J. Gou, D. Gao, Experimental study on the fracture parameters of concrete, Materials (Basel). 14 (2020) 129.

[65] R.F. Gomes, D.P. Dias, F. de Andrade Silva, Determination of the fracture parameters of steel fiber-reinforced geopolymer concrete, Theor. Appl. Fract. Mech. 107 (2020) 102568.

[66] K. Hover, Testing hardened concrete, Aberdeen's Concr. Constr. 38 (1993).

[67] B.A. Zai, M.A. Khan, K.A. Khan, A. Mansoor, A. Shah, M. Shahzad, The role of dynamic response parameters in damage prediction, Proc. Inst. Mech. Eng. Part C J. Mech. Eng. Sci. 233 (2019) 4620–4636.

[68] M. Boltezar, B. Strancar, A. Kuhelj, Identification of transverse crack location in flexural vibrations of free-free beams, J. Sound Vib. 211 (1998) 729–734. https://doi.org/10.1006/jsvi.1997.1410.

[69] M. Akbarzadeh Khorshidi, D. Soltani, Diagnosis of Type, Location and Size of Cracks by Using Generalized Differential Quadrature and Rayleigh Quotient Methods, J. Theor. Appl. Mech. 43 (2013) 61–70. https://doi.org/10.2478/jtam-2013-0006.

[70] S. Moradi, H. Makvandi, D. Poorveis, K.H. Shirazi, Free vibration analysis of cracked postbuckled plate, Appl. Math. Model. 66 (2019) 611–627. https://doi.org/10.1016/j.apm.2018.10.004.

[71] D.K. Agarwalla, D.R. Parhi, Effect of crack on modal parameters of a cantilever beam subjected to vibration, Procedia Eng. 51 (2013) 665–669. https://doi.org/10.1016/j.proeng.2013.01.094.

[72] E. Douka, L.J. Hadjileontiadis, Time-frequency analysis of the free vibration response of a beam with a breathing crack, NDT E Int. 38 (2005) 3–10. https://doi.org/10.1016/j.ndteint.2004.05.004.

[73] S. Ghadimi, S.S. Kourehli, Multiple crack identification in Euler beams using extreme learning machine, KSCE J. Civ. Eng. 21 (2017) 389–396. https://doi.org/10.1007/s12205-016-1078-0.

[74] I. Hager, AN OVERVIEW OF CONCRETE MODULUS OF ELASTICITY EVOLUTION WITH IFireSS – International Fire Safety Symposium, (2015).

[75] N.T. Khiem, N.N. Huyen, A method for crack identification in functionally graded Timoshenko beam, Nondestruct. Test. Eval. 32 (2017) 319–341. https://doi.org/10.1080/10589759.2016.1226304.

[76] K. Mazanoglu, M. Sabuncu, A frequency based algorithm for identification of single and double cracked beams via a statistical approach used in experiment, Mech. Syst. Signal Process. 30 (2012) 168–185. https://doi.org/10.1016/j.ymssp.2012.02.004.

[77] T. Fleet, K. Kamei, F. He, M.A. Khan, K.A. Khan, A. Starr, A machine learning approach to model interdependencies between dynamic response and crack propagation, Sensors

(Switzerland). 20 (2020) 1–13. https://doi.org/10.3390/s20236847.

[78] A. Priyadarshini, Identification of cracks in beams using vibrational analysis, (2013).

[79] Z.A. Jassim, N.N. Ali, F. Mustapha, N.A. Abdul Jalil, A review on the vibration analysis for a damage occurrence of a cantilever beam, Eng. Fail. Anal. 31 (2013) 442–461. https://doi.org/10.1016/j.engfailanal.2013.02.016.

[80] A.N. Hoshyar, B. Samali, R. Liyanapathirana, A.N. Houshyar, Y. Yu, Structural damage detection and localization using a hybrid method and artificial intelligence techniques, Struct. Heal. Monit. 19 (2020) 1507–1523. https://doi.org/10.1177/1475921719887768.

[81] M. Chati, R. Rand, S. Mukherjee, Modal analysis of a cracked beam, J. Sound Vib. 207 (1997) 249–270. https://doi.org/10.1006/jsvi.1997.1099.

[82] G.R. Gillich, H. Furdui, M. Abdel Wahab, Z.I. Korka, A robust damage detection method based on multi-modal analysis in variable temperature conditions, Mech. Syst. Signal Process. 115 (2019) 361–379. https://doi.org/10.1016/j.ymssp.2018.05.037.

[83] G.R. Gillich, Z.I. Praisach, Modal identification and damage detection in beam-like structures using the power spectrum and time-frequency analysis, Signal Processing. 96 (2014) 29–44. https://doi.org/10.1016/j.sigpro.2013.04.027.

[84] A.K. Pandey, M. Biswas, M.M. Samman, Damage Detection From Mode Changes In Curvature, J. Sound Vib. 145 (1991) 321–332. https://doi.org/10.1213/ANE.0000000000001634.

[85] J.A. Loya, L. Rubio, J. Fernández-Sáez, Natural frequencies for bending vibrations of Timoshenko cracked beams, J. Sound Vib. 290 (2006) 640–653. https://doi.org/10.1016/j.jsv.2005.04.005.

[86] G.-R. Gillich, Z.-I. Praisach, M. Abdel Wahab, H. Furdui, A new modal-based damage location indicator, {P}roceedings of the {I}nternational {C}onference on {N}oise and {V}ibration {E}ngineering {ISMA 2014}. (2014) 499–512.

[87] M. Nitesh A., P. Vaibhav S., Analysis of Crack Detection of A Cantilever Beam using Finite Element Analysis, Int. J. Eng. Res. Technol. 4 (2015) 713–718. https://doi.org/10.1002/jpln.200800218.

[88] Y.D. Shinde, S.D. Katekar, Vibration Analysis of Cantilever Beam With Single Crack using Experimental Method, Int. J. Eng. Res. Technol. 3 (2014) 1644–1648.

[89] S. Das, P. Saha, S.K. Patro, Vibration-based damage detection techniques used for health monitoring of structures: a review, J. Civ. Struct. Heal. Monit. 6 (2016) 477–507. https://doi.org/10.1007/s13349-016-0168-5.

[90] A. Gupta, N.K. Jain, R. Salhotra, P.V. Joshi, Effect of thermal environment on vibration analysis of isotropic micro plate with inclined crack based on modified couple stress theory, 24th Int. Congr. Sound Vib. ICSV 2017. (2017) 1–7.

[91] J. Hu, An integrated approach to detection of cracks using vibration characteristics, (n.d.) 841–853.

[92] G.L. Qian, S.N. Gu, J.S. Jiang, The dynamic behaviour and crack detection of a beam with a crack, J. Sound Vib. 138 (1990) 233–243. https://doi.org/10.1016/0022-460X(90)90540-G.

[93] G.R. Gillich, N.M.M. Maia, I.C. Mituletu, Z.I. Praisach, M. Tufoi, I. Negru, Early structural damage assessment by using an improved frequency evaluation algorithm, Lat. Am. J. Solids Struct. 12 (2015) 2311–2329. https://doi.org/10.1590/1679-78251795.

[94] J.H. Haido, B.H.A. Bakar, A.A. Abdul-Razzak, J. Jayaprakash, K.K. Choong, Simulation of

dynamic response for steel fibrous concrete members using new material modeling, Constr. Build. Mater. 25 (2011) 1407–1418.

[95] G.-D. Zhou, T.-H. Yi, A summary review of correlations between temperatures and vibration properties of long-span bridges, Math. Probl. Eng. 2014 (2014).

[96] H. Li, S. Li, J. Ou, H. Li, Modal identification of bridges under varying environmental conditions: temperature and wind effects, Struct. Control Heal. Monit. 17 (2010) 495–512.

[97] Y. Xia, B. Chen, S. Weng, Y.-Q. Ni, Y.-L. Xu, Temperature effect on vibration properties of civil structures: a literature review and case studies, J. Civ. Struct. Heal. Monit. 2 (2012) 29–46.

[98] Y. Xia, Y.-L. Xu, Z.-L. Wei, H.-P. Zhu, X.-Q. Zhou, Variation of structural vibration characteristics versus non-uniform temperature distribution, Eng. Struct. 33 (2011) 146–153.

[99] L. Li, R. Zhang, L. Jin, X. Du, J. Wu, W. Duan, Experimental study on dynamic compressive behavior of steel fiber reinforced concrete at elevated temperatures, Constr. Build. Mater. 210 (2019) 673–684. https://doi.org/10.1016/j.conbuildmat.2019.03.138.

[100] M. Nili, V. Afroughsabet, The long-term compressive strength and durability properties of silica fume fiber-reinforced concrete, Mater. Sci. Eng. A. 531 (2012) 107–111.

[101] V. Nguyen-Van, J. Liu, C. Peng, G. Zhang, H. Nguyen-Xuan, P. Tran, Dynamic responses of bioinspired plastic-reinforced cementitious beams, Cem. Concr. Compos. 133 (2022) 104682.

[102] M. Ekenel, A. Rizzo, J.J. Myers, A. Nanni, Flexural fatigue behavior of reinforced concrete beams strengthened with FRP fabric and precured laminate systems, J. Compos. Constr. 10 (2006) 433–442.

[103] X. Wang, A.M. Sayed, Z. Wu, Modeling of the Flexural Fatigue Capacity of RC Beams Strengthened with FRP Sheets Based on Finite-Element Simulation, J. Struct. Eng. (United States). 141 (2015). https://doi.org/10.1061/(ASCE)ST.1943-541X.0001161.

[104] T. Matsumoto, V.C. Li, Fatigue life analysis of fiber reinforced concrete with a fracture mechanics based model, Cem. Concr. Compos. 21 (1999) 249–261.

[105] J.D. Ríos, H. Cifuentes, Probabilistic fatigue analysis of ultra-high-performance fibre-reinforced concrete under thermal effects, in: MATEC Web Conf., EDP Sciences, 2018: p. 12001.

[106] P. Léger, M. Leclerc, Hydrostatic, Temperature, Time-Displacement Model for Concrete Dams, J. Eng. Mech. 133 (2007) 267–277. https://doi.org/10.1061/(asce)0733-9399(2007)133:3(267).

[107] R.M.L. Foote, Y.-W. Mai, B. Cotterell, Crack growth resistance curves in strain-softening materials, J. Mech. Phys. Solids. 34 (1986) 593–607.

[108] J. Zhang, V.C. Li, Simulation of crack propagation in fiber-reinforced concrete by fracture mechanics, Cem. Concr. Res. 34 (2004) 333–339.

[109] R.C. Van Staden, H. Guan, Y.-C. Loo, Application of the finite element method in dental implant research, Comput. Methods Biomech. Biomed. Engin. 9 (2006) 257–270.

[110] Z.S. Nuguzhinov, Z.B. Bakirov, N.I. Vatin, M.Z. Bakirov, I.A. Kurokhtina, D.T. Tokanov, O. Khabidolda, Stress Intensity Factor of Reinforced Concrete Beams in Bending, Buildings. 11 (2021) 287.

[111] S. Greenland, S.J. Senn, K.J. Rothman, J.B. Carlin, C. Poole, S.N. Goodman, D.G. Altman, Statistical tests, P values, confidence intervals, and power: a guide to misinterpretations, Eur. J. Epidemiol. 31 (2016) 337–350.

2023-01-18

Dynamic response-based crack resistance analysis of fibre reinforced concrete specimens under different temperatures and crack depths

Khalel, Hamad H Zedan

Elsevier

Khalel HHZ, Khan M, Starr A. (2023) Dynamic response-based crack resistance analysis of fibre reinforced concrete specimens under different temperatures and crack depths, Journal of Building Engineering, Volume 66, May 2023, Article Number 105865

https://doi.org/10.1016/j.jobe.2023.105865